

Industrial Indoor Measurements from 2-6 GHz for the 3GPP-NR and QuaDRiGa Channel Model

Stephan Jaeckel*, Nick Turay*, Leszek Raschkowski*, Lars Thiele*, Risto Vuohtoniemi[‡], Marko Sonkki[‡],
Veikko Hovinen[‡], Frank Burkhardt[†], Prasanth Karunakaran[†], and Thomas Heyn[†]

* Fraunhofer Heinrich Hertz Institute, Berlin, Germany, stephan.jaeckel@hhi.fraunhofer.de

[‡] Centre for Wireless Communications, Oulu, Finland

[†] Fraunhofer Institute for Integrated Circuits, Erlangen, Germany

Abstract—Providing reliable low latency wireless links for advanced manufacturing and processing systems is a vision of Industry 4.0. Developing, testing and rating requires accurate models of the radio propagation channel. The current 3GPP-NR model as well as the QuaDRiGa model lack the propagation parameters for the industrial indoor scenario. To close this gap, measurements were conducted at 2.37 GHz and 5.4 GHz at operational Siemens premises in Nuremberg, Germany. Furthermore, the campaign was planned to allow the test and parameterization of new features of the QuaDRiGa channel model such as support for device-to-device (D2D) radio links and spatial consistency. A total of 5.9 km measurement track was used to extract the statistical model parameters for line of sight (LOS) and Non-LOS propagation conditions. It was found that the metallic walls and objects in the halls create a rich scattering environment, where a large number of multipath components arrive at the receiver from all directions. This leads to a robust communication link, provided that the transceivers can handle the interference. The extracted parameters can be used in geometric-stochastic channel models such as QuaDRiGa to support simulation studies, both on link and system level.

I. INTRODUCTION

The tremendous developments in the fields of electronics, communication, and advanced manufacturing in the past years are leading to a shift from digital to intelligent production methods in manufacturing companies [1]. This modernization in manufacturing is based on the integration of new technologies into a cyber-physical system commonly known as Industry 4.0. The aim of Industry 4.0 is to establish a highly flexible production model of customized products and services where realtime interactions between humans, products, and devices during the production process are feasible [2]. One technology that is often discussed in this context is D2D communication. It offers new ways to communicate with less latency, transfer large amounts of data, and reduce the load in the core network [3].

Geometry-based stochastic channel models (GSCMs) such as the 3rd generation partnership project (3GPP) new radio (NR) model [4] and the QuaDRiGa channel model [5] offer efficient ways to evaluate the performance of mobile wireless communication systems during standardization and before product development stages. These models emulate the wireless propagation environment by clearly defined stochastic processes, but the interactions of transmitters (TXs) and receivers (RXs) with this randomized environment are purely

deterministic and predictable. This approach drastically reduces the complexity compared to, e.g., ray tracing, but it requires parameterization to emulate the wireless propagation environment correctly. Finding the model parameters is a labor intensive and time consuming task. One approach is to use fully deterministic models such as ray tracing to determine the GSCM parameters. Another way is to perform channel sounding measurements in a real environment and then extract the model parameters from the recorded channel impulse responses (CIRs). This has been done for many outdoor (e.g., [6], [7]) and some office type scenarios (e.g., [8]). So far, the 3GPP community has focussed on outdoor environments and some office type scenarios [4]. Additional extensions cover vehicle-to-everything [9], non-terrestrial networks [10], and aerial vehicles [11]. However, the influence of an industrial production environment on the radio transmission, both for D2D as well as infrastructure-based systems, is not well understood and the corresponding GSCM parameters are missing. To close this gap, we performed radio channel measurements in five different factory halls at operational Siemens premises in Nuremberg, Germany. The measurements were done at 2.37 GHz and 5.4 GHz, covered a total of 5.9 km indoor measurement tracks, and led to more than 5,000 data-points for all relevant parameters. The results allow the use of the 3GPP and QuaDRiGa channel models for industrial systems in a frequency range from 2 GHz to 6 GHz and thus enable more accurate simulation studies for fifth generation (5G) and beyond-5G wireless communications systems. This is especially relevant for so-called private campus networks which will be deployed at around 3.5 GHz in many countries.

II. MEASUREMENTS

Measurements were done in an industrial indoor environment within five different factory halls in Nuremberg, Germany. The halls show different properties with regard to geometry, structure and installed objects. This leads to different propagation conditions and a different behavior of the signal transmission within each hall. Several measurement tracks were defined along which a transceiver unit was moved accordingly, as depicted in Figure 3. An arrow symbolizes the TX position in the single mobility scenario and the black lines indicate the measurement tracks. Start and end points are represented by a white circle. The exact position information

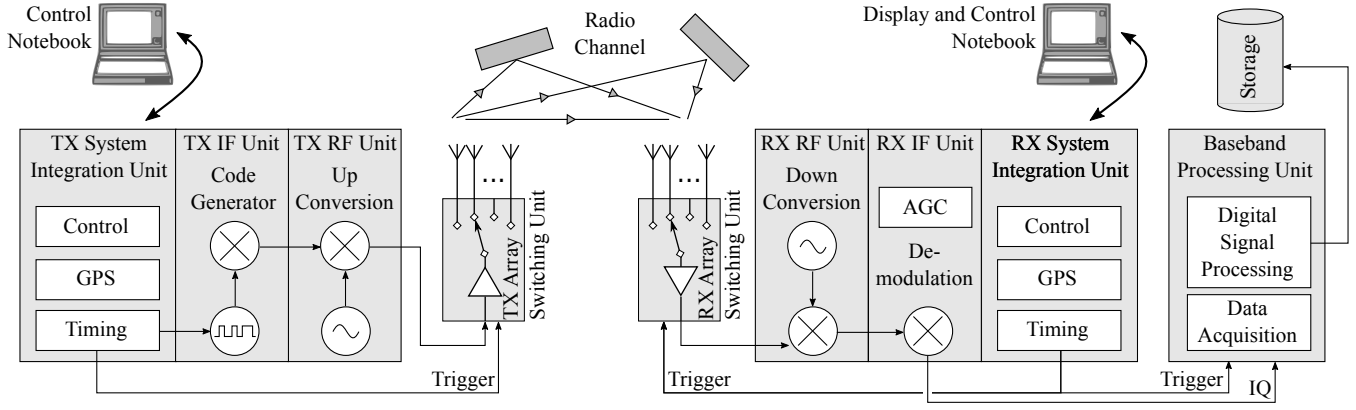


Fig. 1. Propsound channel sounder architecture

of the TX and RX during the recording was measured using a laser ranger and a distance wheel. The RX antenna height was always set to approx. 2 m whereas the TX height was varied from 2 m to 8 m to cover different deployment scenarios. For example, two machines might communicate with each other when they are moving around in the factory. In this dual mobility scenario, both are at a height of 2 m. The fixed communication infrastructure, on the other hand, might be installed under the roof of the factory at a height of 6 m or 8 m. The majority of measurements were done at a variable distance between the TX and the RX by either moving the RX (single mobility) or both the RX and the TX units (dual mobility). To study the influence of the LOS propagation, roughly 1/3 of the measurements were done in LOS conditions and 2/3 were in non-line of sight (NLOS) conditions. The measurements were done at distances ranging from 5 m to 150 m for both LOS and NLOS channels. A total of 208 tracks were measured, resulting in a total of 5.9 km measurement tracks. An overview of the measurement parameters is given in Table I.

A wideband Propsound channel sounder was used to capture the in-phase and quadrature (IQ) data. To avoid interfering the factory processes, and to ensure an interference free data capture, the radio frequency (RF) spectrum was constantly screened for interference. In addition, the transceiver system was calibrated before and after the measurements were carried

out to minimize the systems influence on the captured data. The architecture of the Propsound channel sounder is depicted in Figure 1. Both the TX and the RX unit use an intermediate frequency (IF) of 1.45 GHz which is connected to customized RF units for different frequency bands. The TX generates a wideband pseudo random binary phase-shift keying (BPSK) signal using a direct sequence spread spectrum approach. The BPSK signal is modulated onto the desired carrier frequency in the TX unit and down converted back to the IF at the RX. A system integration unit contains all control functions, timing, synchronization, and interfaces to other units.

Array antennas are used to extract information about the spatial signal properties (e.g., the angles of departure and arrival). The antenna elements are sequentially switched to measure the whole multiple-input multiple-output (MIMO) channel matrix. Hence, only a single TX-RX antenna pair is active at any given time. The TX array element selection is held constant while the RX switches through all available elements. When the RX cycle is complete, the TX switches to the next element and the RX antenna switching cycle repeats. The array antennas are depicted in Figure 2. They are constructed from dual-polarized patch elements with a half power beamwidth of 70°. The polarization angles are $\pm 45^\circ$ with respect to the vertical which helps to preserve the signal strength of the final θ (vertical) and ϕ (horizontal) polarizations in manmade environments dominated by horizontal and vertical surfaces. All antennas were calibrated via measurements in an anechoic chamber. The characterization of the antenna patterns is mandatory to correctly estimate the arrival and departure angles. The measurement settings and additional auxiliary information are time tagged and embedded in the recorded data. These are later used for post processing.

The measurements were done at two different carrier frequencies: 5.4 GHz (200 MHz bandwidth) and 2.37 GHz (50 MHz bandwidth). In both cases, the bandwidth is sufficient to extract the channel model parameters using high resolution algorithms such as [12]. To be able to interpolate between the two frequencies with regards to radio propagation behaviour, the measurement conditions for both frequency were kept very similar, e.g., the same measurement tracks and transmitter

TABLE I
MEASUREMENT PARAMETERS

Parameter	Setup 1	Setup 2	Setup 3
Center Frequency	5.4 GHz		2.37 GHz
Bandwidth	200 MHz		50 MHz
TX power	23 dBm		13 dBm
Noise floor	-101.3 dBm		-102.7 dBm
Max. CIR length	4.2 μ s		4.6 μ s
TX Antenna Config.	ODA	Cross	Planar
No. TX elements	32	30	32
TX element gain	7.9 dBi	8.1 dBi	8.2 dBi
TX array aperture	205°	90°	90°
RX Antenna Config.	ODA		ODA
No. RX elements	50		56
RX element gain	8.0 dBi		7.2 dBi
RX array aperture	360°		360°

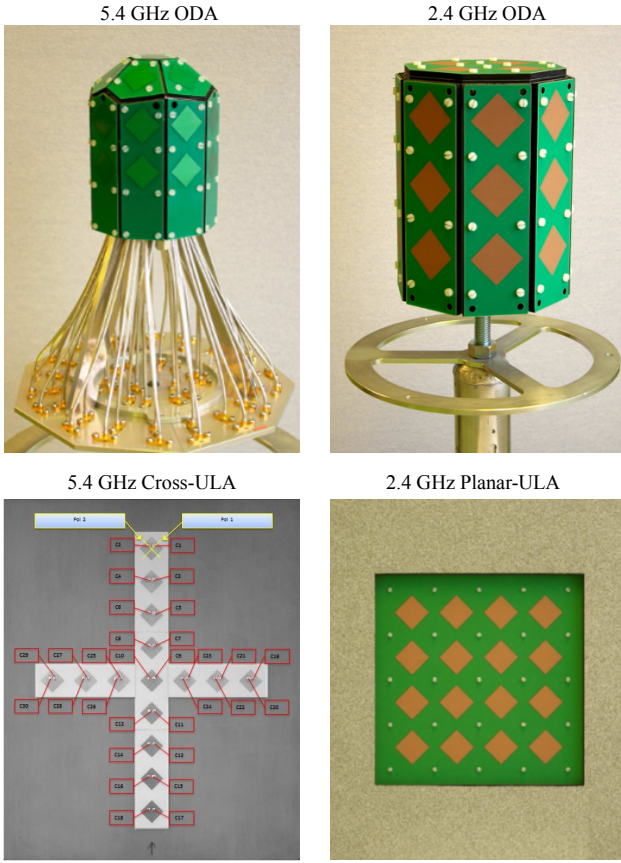


Fig. 2. Measurement antennas

heights were used during the recordings. However, there are differences in the antenna configurations used depending on the frequency. This leads to some restrictions regarding data analysis. The three measurement setups are as follows:

Setup 1 - 5.4 GHz, TX-ODA, RX-ODA configuration:

This configuration was used when both the TX and the RX were mobile. The TX was equipped with an omni directional array (ODA) consisting of 16 dual-polarized elements covering an azimuth range of 205° . This is sufficient to calculate the azimuth angle spreads at the transmitter. The RX used a 25-element dual-polarized ODA that covered the whole sphere, i.e., it is possible to resolve paths from all directions.

Setup 2 - 5.4 GHz TX-Cross-ULA, RX-ODA configuration:

For scenarios that included a stationary transmitter, the TX used an uniform linear array (ULA) with 15 dual-polarized elements arranged in a planar (cross shaped) fashion. The antenna can resolve departure angles within $\pm 45^\circ$ relative to the antenna broadside. This is sufficient for the elevation direction, where there are no significant scatterers directly above or below the antenna. During the measurement planning, it was assumed that no significant paths would arrive from the rear of the antenna. However, during the data analysis it was found that the metal hall creates a rich scattering environment where the direction of many propagation paths exceeded the 90° range. This had to be considered during the data analysis.

Setup 3 - 2.37 GHz TX-Planar-ULA, RX-ODA configuration:

A planar TX antenna arrangement was used for all measurements at 2.37 GHz. Here the TX array consists of 16 dual-polarized elements and the RX array uses 28 dual-polarized elements. The same limitations as for the 5.4 GHz TX-Cross-ULA apply, i.e., the departure angles can be estimated within $\pm 45^\circ$ relative to the antenna broadside. However, results from Setup 3 are comparable to Setup 2 since the measurements were done using identical transceiver positions and very similar antenna configurations.

During the measurements, the complete MIMO channel, i.e., the broadband channel response of all TX-RX antenna pairs, was sampled every few centimeters. One such characterization of the channel is called a *snapshot*. The first post processing step is to derive the *path parameters*, i.e., the path powers, delays and angles of the multipath components (MPCs) from the channel snapshots. The path parameters (delay, power, angles, and polarization) are estimated from the raw measurement data by an estimation method similar to the SAGE algorithm (Space Alternating Generalized Expectation Maximization) [12]. However, the procedure used in this paper is divided into two steps. First, the path delay and the MIMO coefficient matrix are calculated for each MPC. This step is independent of the antennas. Then, in a second step, the departure and arrival angles are calculated. The algorithm is described in [13]. The next step is to calculate the large-scale parameters (LSPs). The complete list of parameters consists of

- the path loss (PL) and shadow fading (SF),
- the Ricean K-factor (KF),
- the root mean square (RMS) delay spread (DS),
- the RMS azimuth spread of arrival (ASA),
- the RMS azimuth spread of departure (ASD),
- the RMS elevation spread of arrival (ESA),
- the RMS elevation spread of departure (ESD), and
- the cross polarization ratio (XPR).

Small-scale-fading (SSF), fast fluctuations of the power of a MPC, can lead to strong fluctuations of these parameters even in subsequent snapshots. For example, different DS values might be calculated from two successive snapshots, even if they were measured only centimeters away from each other. To reduce this effect, Jalden *et al.* [14] suggested to average the results within a certain radius. Here, this *averaging interval* was set to 1 m for a good balance between the reduction of SSF effects and the number of measurement samples available for further analysis. For example, a typical measurement track has a length of about 60 m. With one snapshot per wavelength, a total of 700 snapshots is captured for this track. The track is split into 60 *averaging intervals*, each containing 12 snapshots. The LSPs are calculated for each snapshot and are averaged within the interval - leading to 60 values for the DS, the KF, the SF, and so on. In this way, 5,468 sample points were obtained from the whole measurements. The dependency of the parameters on the TX-RX distance, the TX height, and the carrier frequency was evaluated. The results of this evaluation are presented and discussed in the following section.

III. RESULTS AND DISCUSSION

Based on the distance, TX height, and frequency, there are eight variables that describe the distribution of a LSP. These variables are

- 1) the reference value μ (μ) at 1 GHz, 1 m distance, and 1 m TX height,
- 2) the reference standard deviation (STD) σ (σ) at 1 GHz, 1 m distance, and 1 m TX height,
- 3) the decorrelation distance λ (λ) in meters,
- 4) the frequency dependence γ (γ) of the reference value scaling with $\log_{10}(f_{\text{GHz}})$,
- 5) the distance dependence ϵ (ϵ) of the reference value scaling with $\log_{10}(d_{2D})$,
- 6) the height dependence ζ (ζ) of the reference value scaling with $\log_{10}(h_{\text{TX}})$,
- 7) the frequency dependence δ (δ) of the reference STD scaling with $\log_{10}(f_{\text{GHz}})$,
- 8) the distance dependence κ (κ) of the reference STD scaling with $\log_{10}(d_{2D})$.

These parameters are used in GSCMs such as the QuaDRiGa model or the 3GPP-NR model [4] to generate artificial channel coefficients for simulation studies. The values V of a LSP are calculated by

$$V = V_{\mu} + V_{\gamma} \cdot \log_{10} f_{\text{GHz}} + V_{\epsilon} \cdot \log_{10} d_{2D} + V_{\zeta} \cdot \log_{10} h_{\text{BS}} + X(V_{\sigma} + V_{\delta} \cdot \log_{10} f_{\text{GHz}} + V_{\kappa} \cdot \log_{10} d_{2D}), \quad (1)$$

where X is a Normal distributed random variables having zero-mean and unit variance. Likewise, the measurements are analyzed by fitting this formula to the more than 5,000 data points. The measurement tracks were separated into LOS and NLOS and the parameters were fitted for the three measurement setups independently as well as for the combined dataset¹. The analysis results are shown in Table II. As a reference, the last columns in the table contain the parameters of the popular 3GPP 38.901 indoor office scenario [4]. These values also have been used in industrial settings in the past due to the lack of consolidated parameters for the industrial indoor scenario. In the following, the analysis results are discussed.

A. Large-Scale Parameters

Path loss (PL): The PL depends on the 2D distance (i.e., the distance on the ground) between TX and RX and the carrier frequency. A dependence on the TX height was not found. For both LOS and NLOS, results are close to the free space PL. For the NLOS case, it means that there is strong coverage with high power despite the lack of a direct LOS path. The 5.4 GHz measurements have 7 dB less power compared to the 2.37 GHz measurements. This is consistent with the theory of free-space propagation where the received power scales with the square of the frequency (i.e., 7.15 dB less power at 5.4 GHz compared to 2.37 GHz). Compared to 3GPP indoor office, there is a

¹The combined parameters in Table II were obtained by fitting (1) to a combination of datapoints from the measurements, not averaging the values from the individual setups.

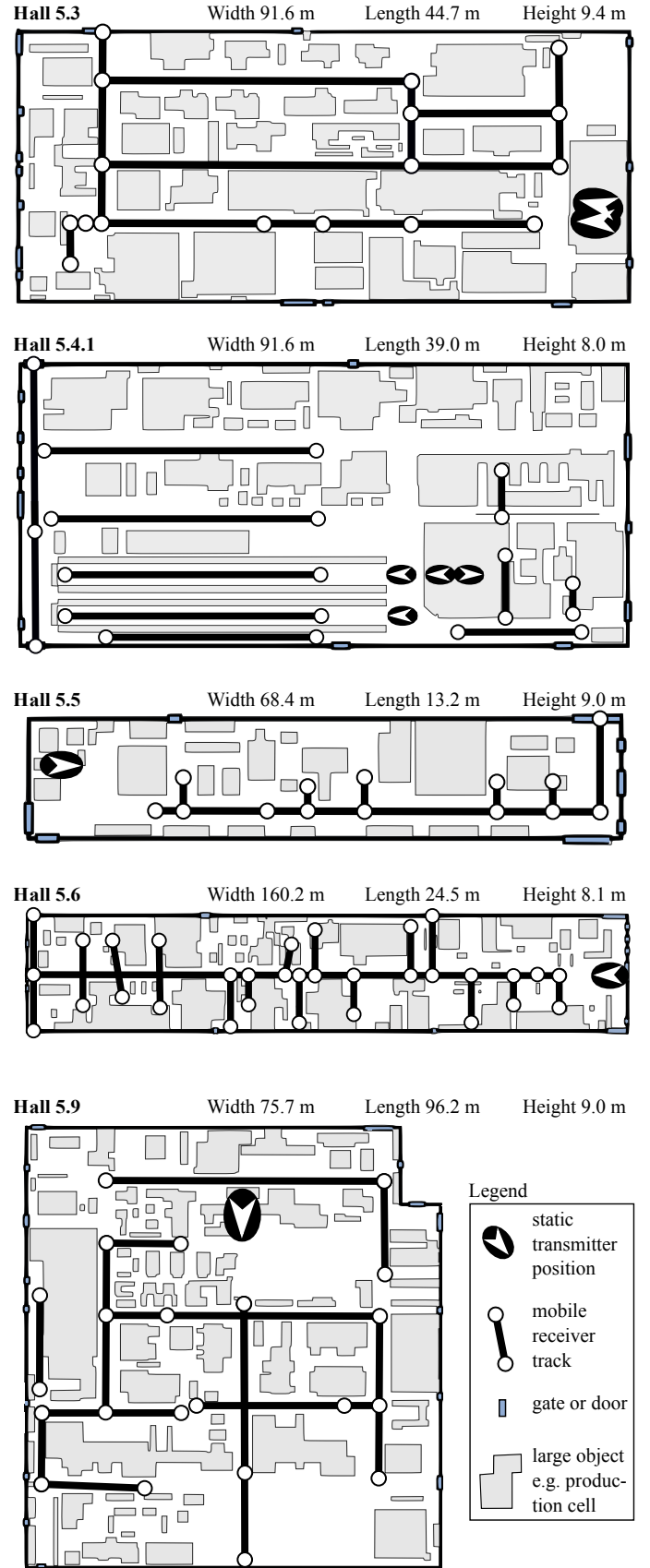


Fig. 3. Floor plans of the five measurement halls

TABLE II
INDUSTRIAL LARGE-SCALE PARAMETERS

Parameter	Unit		Setup 1		Setup 2		Setup 3		Combined		3GPP 38.901	
			5.4 GHz, TX-ODA		5.4 GHz TX-Cross		2.37 GHz TX-Planar		Indoor Industrial		Indoor Office	
			LOS	NLOS	LOS	NLOS	LOS	NLOS	LOS	NLOS	LOS	NLOS
PL	dB	PL_{μ}	36.1	34.4	34.3	39.2	37.2	30.1	36.3	29.1	32.4	17.3
Shadow Fading	dB	PL_{σ}	1.6	1.6	1.5	3.1	1.7	1.7	1.8	1.15	3.0	8.0
SF decorr. dist.	m	SF_{λ}	20.6	8.0	3.5	34.2	14.8	32.1	15.0	30.0	10.0	6.0
PL freq. dep.	dB/log10(GHz)	PL_{γ}	20	20	20	20	20	20	19.5	25.4	20.0	24.9
PL dist. dep.	dB/log10(m)	PL_{ϵ}	18.5	21.7	19.3	21.7	17.6	24.7	18.3	24.1	17.3	38.3
SF freq. dep.	dB/log10(GHz)	SF_{δ}	0	0	0	0	0	0	-0.3	3.15	0	0
DS	log10(s)	DS_{μ}	-7.22	-7.12	-7.47	-7.19	-7.78	-7.72	-8.3	-8.19	-7.69	-7.17
DS STD	log10(s)	DS_{σ}	0.08	0.08	0.14	0.09	0.11	0.12	0.09	0.11	0.18	0.055
DS decorr. dist.	m	DS_{λ}	42.1	36.4	24.2	10.5	99.7	127.2	50.0	52.0	8.0	5.0
DS freq. dep.	log10(s)/log10(GHz)	DS_{γ}	0	0	0	0	0	0	1.26	1.37	-0.01	-0.28
DS height dep.	log10(s)/log10(m)	DS_{ζ}	0.36	0.31	0.56	0.17	0.4	0.38	0.49	0.3	0	0
DS STD freq. dep.	log10(s)/log10(GHz)	DS_{δ}	0	0	0	0	0	0	0.07	0	0	0.1
Delay Factor		r_{DS}	2.93	3.03	2.56	2.89	2.55	2.74	2.7	3.0	3.6	3.0
KF	dB	KF_{μ}	-1.6	-4.0	4.8	-4.4	2.8	-1.0	7.8	4.2	7.0	N/A
KF STD	dB	KF_{σ}	2.7	2.5	2.9	2.4	2.6	1.9	1.8	1.1	4.0	N/A
KF decorr. dist.	m	KF_{λ}	17.5	11.4	13.5	6.1	30.3	17.0	32.0	14.0	4.0	N/A
KF freq. dep.	dB/log10(GHz)	KF_{γ}	0	0	0	0	0	0	-7.3	-11.7	0	N/A
KF height dep.	dB/log10(m)	KF_{ζ}	-5.7	-6.3	-8.2	-1.0	-3.6	-1.9	-7.7	-3.3	0	N/A
KF STD freq. dep.	dB/log10(GHz)	KF_{δ}	0	0	0	0	0	0	2.6	2.2	0	N/A
ASA	log10(°)	ASA_{μ}	1.67	1.61	1.71	1.61	1.67	1.56	1.69	1.62	1.781	1.863
ASA STD	log10(°)	ASA_{σ}	0.15	0.18	0.12	0.2	0.19	0.26	0.15	0.22	0.119	0.059
ASA decorr. dist.	m	ASA_{λ}	6.1	6.8	12.1	9.5	6.3	9.8	10.0	13.0	5.0	3.0
ASA freq. dep.	log10(°)/log10(GHz)	ASA_{γ}	0	0	0	0	0	0	0	0	-0.19	-0.11
ASA STD freq. dep.	log10(°)/log10(GHz)	ASA_{δ}	0	0	0	0	0	0	0	0	0.12	0.12
ASD	log10(°)	ASD_{μ}	1.54	1.64	-0.06	0.14	0.56	0.75	1.66	1.68	1.60	1.62
ASD STD	log10(°)	ASD_{σ}	0.1	0.1	0.31	0.29	0.32	0.24	0.12	0.1	0.18	0.25
ASD decorr. dist.	m	ASD_{λ}	12.8	16.4	18.1	18.2	23.8	17.9	10.0	13.0	7.0	3.0
ASD height dep.	log10(°)/log10(m)	ASD_{ζ}	0.05	-0.24	1.02	1.43	0.22	0.29	0.1	-0.2	0	0
ESA	log10(°)	ESA_{μ}	1.61	1.72	1.69	1.19	1.71	1.82	1.64	1.64	1.44	1.387
ESA STD	log10(°)	ESA_{σ}	0.07	-0.11	-0.1	0.25	0.09	-0.12	0.01	0.06	0.264	0.746
ESA decorr. dist.	m	ESA_{λ}	13.3	11.4	6.4	12.9	10.3	21.1	10.0	20.0	4.0	4.0
ESA freq. dep.	log10(°)/log10(GHz)	ESA_{γ}	0	0	0	0	0	0	0	0	-0.26	-0.15
ESA dist. dep.	log10(°)/log10(m)	ESA_{ϵ}	-0.5	-0.54	-0.53	-0.34	-0.54	-0.65	-0.5	-0.5	0	0
ESA STD freq. dep.	log10(°)/log10(GHz)	ESA_{δ}	0	0	0	0	0	0	0	0	-0.04	-0.09
ESA STD dist. dep.	log10(°)/log10(m)	ESA_{κ}	0.04	0.15	0.14	0	0.05	0.21	0.09	0.1	0	0
ESD	log10(°)	ESD_{μ}	1.17	1.03	1.4	0.9	1.03	1.43	1.55	1.6	2.228	1.08
ESD STD	log10(°)	ESD_{σ}	0.07	0.1	0.08	0.3	0.08	0.06	0.01	0.17	0.30	0.36
ESD decorr. dist.	m	ESD_{λ}	9.2	12.5	10.4	12.4	6.4	11.6	10.0	20.0	4.0	4.0
ESD freq. dep.	log10(°)/log10(GHz)	ESD_{γ}	0	0	0	0	0	0	0	0	-1.43	0
ESD dist. dep.	log10(°)/log10(m)	ESD_{ϵ}	0	0.16	-0.53	-0.38	-0.2	-0.5	-0.5	-0.5	0	0
ESD height dep.	log10(°)/log10(m)	ESD_{ζ}	0.13	0	0.3	0.54	0.26	0.25	0.3	0.14	0	0
ESD STD freq. dep.	log10(°)/log10(GHz)	ESD_{δ}	0	0	0	0	0	0	0	0	0.13	0
ESD STD dist. dep.	log10(°)/log10(m)	ESD_{κ}	0	-0.03	0.05	-0.08	0.08	0.08	0.09	0.1	0	0
XPR	dB	XPR_{μ}	13.0	12.8	18.0	15.2	16.1	15.0	16.8	14.4	11.0	10.0
XPR STD	dB	XPR_{σ}	1.6	1.3	2.6	1.8	3.2	2.1	3.1	2.4	4.0	4.0
XPR decorr. dist.	m	XPR_{λ}	16.5	7.1	23.4	6.9	14.9	16.3	30.0	27.0	0	0
XPR height dep.	dB/log10(m)	XPR_{ζ}	-1.9	-2.5	-3.6	0.6	-3.5	-3.7	-4.5	-2.2	0	0

6 dB increased LOS-PL in the industrial scenario². This might come from the dimensions of the hall where reflected paths travel a longer distance compared to the office scenario. Also, there was a significant ground reflection in some measured trajectories which effected the average received power due to destructive interference. The NLOS-PL is very different from the 3GPP office model, where there is a 12 dB lower PL in the measured industrial NLOS scenario³. This indicates that the walls and objects in the factory reflect and scatter a significant portion of the transmitted signal.

Shadow fading (SF): SF occurs when an obstacle gets positioned between the TX and the RX. This leads to a reduction in signal strength because the wave is shadowed

or blocked by the obstacle. This is modeled by log-normal distributed with three parameters: the reference STD SF_{σ} defines the width of the distribution, i.e., the power value (in dB) above or below the PL at 1 GHz; the frequency dependence SF_{δ} describes how the SF changes with frequency; and the decorrelation distance SF_{λ} defines how fast the SF varies when the terminal moves through the environment. The SF values are significantly smaller compared to the 3GPP office environment. This also indicates that there might be good coverage due to a large number of reflected paths.

Delay spread (DS): The DS is an important single measure for the delay time extent of a multipath radio channel. It is defined as the square root of the second central moment of the power-delay profile. As for the SF, the decorrelation distance DS_{λ} defines how fast the DS varies when the terminal

²LOS @ 3.5 GHz, 50 m dist.: 78 dB for industrial, 72.6 dB for office

³NLOS @ 3.5 GHz, 50 m dist.: 83.9 dB for industrial, 95.9 dB for office

moves through the environment. The DS is calculated from both the delays τ and the path powers P , i.e., larger DSs can either be achieved by increasing the values of τ and keeping P fixed or adjusting P and keeping τ fixed. To avoid this ambiguity, an additional proportionality factor (delay factor) r_τ is introduced to scale the width of the distribution of τ . In the measurements, the DS increases with increasing TX height and increasing frequency. The measurements at 2.37 GHz have an average DS of around 30 ns whereas at 5.4 GHz, values around 80 ns are measured. These results are independent of the LOS conditions. The 3GPP office scenario assumes values around 50 ns for NLOS and 20 ns for LOS.

Ricean K-factor (KF): The KF is the ratio between the power of the direct path and the power of further, scattered, paths⁴. The KF is assumed to be log-normal distributed defined by its mean value KF_μ , its STD KF_σ , the decorrelation distance KF_λ , and additional height and frequency-dependent terms. In the measurement data, the KF depends on the TX height, where for increasing height, the KF decreases. This is consistent with the DS results: an elevated TX position leads to a larger number of scattered paths in the factory hall, and thus the relative strength of the direct path decreases. However, there are differences between the configurations. In case of Setup 1, at a TX height of 2 m, the KF is only -3 dB⁵, which means that the direct path carries 1/3 of the total received power. In contrast, Setups 2⁶ and 3⁷ show different results at the same TX height of 2 m. For both configurations, approximately 2/3 of the total received energy is carried by the LOS component. In the NLOS scenario there is a LOS-like path, i.e., a path that arrives within 5 ns of the expected LOS arrival time that carries between 15% and 50% of the total received power. This explains the similar PL and DS results when comparing the LOS and NLOS measurements.

Azimuth spread of arrival (ASA): The ASA does not depend on the distance or TX height. Measured values vary between 10 and 90 degree in both LOS and NLOS conditions. This means that signals arrive at the receiver from almost all directions. The averages observed can be found around 40° to 50° (5.4 GHz) and 40° (2.37 GHz). The 3GPP office shows similar values with a slightly smaller ASA for LOS channels which might be due to the increased KF.

Azimuth spread of departure (ASD): If both the TX and the RX are at the same (2 m) height, the ASD is expected to have the same values as the ASA. For Setup 1, the values are around 35°, which is slightly smaller than the expected ASA value of 50°. This might be caused by the smaller TX antenna aperture of 205° which omits paths at the rear side of the antenna. Also, there is a dependence on the TX height for NLOS channels, leading to lower ASD values at higher TX positions. For the other two setups, the measured ASD is much

smaller at values below 5° for both configurations. This is due to the limited aperture of the transmit antennas. Hence, these low values have not been used for the combined industrial scenario. To obtain a consistent combination of the results for D2D applications, the ASD at 2 m TX height must be identical to the ASA at 2 m RX height. Hence, the combined results in Table II take this into account by including the ASA results in the ASD evaluations at 2 m TX height.

Elevation spread of arrival (ESA): The values of the ESA decrease with increasing distance between TX and RX for all of the three antenna array configuration. This might be due to strong reflections at the ground and the roof of the factory hall. The incident angle at the reflector (i.e., at ground and roof) decreases with larger distances and so does the angle spread at the receiver. This is not considered by the 3GPP office scenario, but seems to be relevant for industrial systems.

Elevation spread of departure (ESD): The ESD depends on both the TX-RX distance and the TX height. For Setup 1, there is a height dependency for LOS channels, where the elevation spread increases with increasing TX height, but no distance dependency is observed. This effect does not occur in NLOS channels where the ESD increases with increasing TX-RX distance. At close TX-RX distances, the results agree well with the ESA where both ESA and ESD have values around 15°. However, the ESD is much larger at large distances compared to the ESA. The results from Setup 2 increase with increasing TX height and decrease with increasing distance. The distance dependency is consistent with the Setup 2 and 3 ESA results, but contradicts the Setup 1 results that show an increase in ESD with increasing distance. The contradictions in the results might be explained by the limited TX antenna aperture. To obtain a consistent combination of the results for D2D applications, the ESD at 2 m TX height must be identical to the ESA at 2 m RX height. Hence, the combined results in Table II take this into account by including the ESA results in the ESD evaluations at 2 m TX height.

Cross polarization ratio (XPR): The XPR defines how the polarization changes for a multipath component, i.e., the initial polarization of a path is defined by the transmit antenna. However, for the NLOS components, the transmitted signal undergoes diffraction, reflection or scattering before reaching the receiver. The XPR (in dB) is assumed to be normal distributed. The cross polarization shows values between 13 dB and 16 dB for the 5.4 GHz measurements and a value of 13 dB in case of 2.37 GHz. The high values indicate that the polarization remains almost unchanged for reflected waves. This is consistent with the 3GPP office scenario.

B. Inter-Parameter Correlations

The correlation values between the different parameters are listed in Table III. The upper right part (shown in white) contains the values for the LOS channels, the lower left part shows the values for the NLOS channels. The KF is negatively correlated with the DS, ASA, ASD, ESD and ESA and positively correlated with the SF and the XPR. The DS is positively correlated with the angular spreads. Azimuth and

⁴The KF can also be substantially large in NLOS conditions, if there is a dominant specular path and diffuse scattered paths. This explains the results of the LOS-like path in the measurements.

⁵Setup 1: $KF = -1.6 - 5.7 \cdot \log_{10}(2) \approx -3.3$ dB

⁶Setup 2: $KF = 4.8 - 8.2 \cdot \log_{10}(2) \approx 2.3$ dB

⁷Setup 3: $KF = 2.8 - 3.6 \cdot \log_{10}(2) \approx 1.7$ dB

elevation spreads are positively correlated, both at the TX and at the RX. The ESD is correlated with the ESA, whereas the ASD and the ASA are uncorrelated. This could mean that there is a specular reflection or a single scatterer either on the floor or on the ceiling of the factory hall that increases the elevation spread at both ends of the link simultaneously. But this does not affect the scattering in the azimuth plane.

TABLE III
INTER-PARAMETER CORRELATION VALUES

Inter-Parameter Correlations		L O S							
		DS	KF	SF	ASD	ASA	ESD	ESA	XPR
DS	5.4 ODA	1	-0.57	-0.3	-0.14	0	0	0.32	-0.18
	5.4 Cross	1	-0.75	-0.25	0.17	-0.16	0.3	0.16	-0.5
	2.4 Planar	1	-0.72	-0.03	0.44	0.19	0.4	0.47	-0.33
	Combined	1	-0.7	-0.3	0.4	0	0.4	0.3	-0.4
	3GPP Office	1	-0.5	-0.8	0.6	0.8	0.1	0.2	N/A
KF	5.4 ODA	-0.72	1	0.44	-0.08	0	0.07	-0.4	0.22
	5.4 Cross	-0.46	1	0.38	-0.4	0.08	-0.31	-0.16	0.49
	2.4 Planar	-0.69	1	0.22	-0.55	-0.1	-0.26	-0.3	0.37
	Combined	-0.6	1	0.4	-0.5	0	-0.3	-0.3	0.5
	3GPP Office	N/A	1	0.5	0	0	0	0.1	N/A
SF	5.4 ODA	0.3	0.39	1	0.28	0.12	0.21	0.05	0.2
	5.4 Cross	0.03	0.31	1	-0.05	-0.22	-0.13	-0.18	0.02
	2.4 Planar	0.39	-0.14	1	-0.1	0.03	0.05	0.1	-0.12
	Combined	0.4	0	1	0	0	0	0	0
	3GPP Office	-0.5	N/A	1	-0.4	-0.5	0.2	0.3	N/A
ASD	5.4 ODA	0.07	-0.08	0.11	1	-0.12	0.08	0.34	0.28
	5.4 Cross	-0.41	0.15	0	1	-0.02	0.35	0.15	-0.47
	2.4 Planar	0.3	-0.22	0	1	0	0.3	0.26	-0.41
	Combined	0.2	0	0.2	1	0	0.4	0.2	-0.5
	3GPP Office	0.4	N/A	0	1	0.4	0.5	0	N/A
ASA	5.4 ODA	-0.35	0.19	0.14	0	1	0.15	-0.13	0.07
	5.4 Cross	0.11	-0.04	0.44	-0.18	1	0.16	0.33	0.26
	2.4 Planar	0.3	-0.03	0.31	0.06	1	0.12	0.43	-0.1
	Combined	0	0	0.2	0	1	0.1	0.3	0
	3GPP Office	0	N/A	-0.4	0	1	0	0.5	N/A
ESD	5.4 ODA	0	-0.12	-0.21	0	-0.07	1	0.06	0.23
	5.4 Cross	0	0	0.29	0.04	0.27	1	0.52	-0.24
	2.4 Planar	0.45	-0.34	0.19	0.35	0	1	0.31	-0.04
	Combined	0.3	-0.3	0.3	0.4	0	1	0.3	-0.2
	3GPP Office	-0.27	N/A	0	0.35	-0.08	1	0	N/A
ESA	5.4 ODA	0	0.04	0.14	-0.19	0.19	-0.1	1	-0.05
	5.4 Cross	0.03	0.08	0.37	-0.18	0.31	0.17	1	-0.1
	2.4 Planar	0.5	-0.26	0.22	0.05	0.44	0.19	1	-0.22
	Combined	0.3	0	0.3	0	0.3	0.3	1	-0.2
	3GPP Office	-0.06	N/A	0	0.23	0.43	0.42	1	N/A
XPR	5.4 ODA	-0.36	0.26	0	-0.08	0.04	0.04	0	1
	5.4 Cross	0.12	0.02	0.14	-0.16	0.23	0.06	0.06	1
	2.4 Planar	-0.43	0.27	-0.07	-0.27	-0.07	-0.32	-0.3	1
	Combined	-0.4	0.3	0	-0.2	0	0	-0.3	1
	3GPP Office	N/A	N/A	N/A	N/A	N/A	N/A	N/A	1

IV. CONCLUSIONS

We performed several measurements under different typical industrial scenarios and conditions in various production halls with different topologies. The measurement data was processed and used to iteratively calculate the corresponding parameters that can be used in the 3GPP-NR channel model and the QuaDRiGa model. The outcome of our work is a propagations channel model that is able to describe radio propagation behavior in automation industry halls for typical industrial settings. In addition the model supports application cases like automatic guided vehicles and D2D communication in machine production halls. An open-source implementation of that model can be found at [5].

ACKNOWLEDGEMENT

The authors thank the Celtic Office and national funding authorities BMBF in Germany, Business Finland, and MINETAD in Spain for supporting this research and development through the ReICOvAir project. The project benefited also from the valuable technical contributions from GHMT AG, CETECOM GmbH, and Qosmotec GmbH in Germany; Trimek S.A. and SQS S.A. in Spain; Verkotan Ltd., Kaltio Technologies, and Sapotech in Finland. This research was also supported in part by the Academy of Finland 6Genesis Flagship (grant no. 318927).

REFERENCES

- [1] B. Chen, J. Wan, L. Shu, P. Li, M. Mukherjee, and B. Yin, "Smart factory of industry 4.0: Key technologies, application case, and challenges," *IEEE Access*, vol. 6, pp. 6505–6519, 2018.
- [2] K. Zhou, Taigang Liu, and Lifeng Zhou, "Industry 4.0: Towards future industrial opportunities and challenges," in *2015 12th International Conference on Fuzzy Systems and Knowledge Discovery (FSKD)*, Aug 2015, pp. 2147–2152.
- [3] A. Asadi, Q. Wang, and V. Mancuso, "A survey on device-to-device communication in cellular networks," *IEEE Communications Surveys & Tutorials*, vol. 16, no. 4, pp. 1801–1819, 2014.
- [4] 3GPP TR 38.901 v15.0.0, "Study on channel model for frequencies from 0.5 to 100 GHz," Tech. Rep., 2018.
- [5] [Online]. Available: <http://www.quadriga-channel-model.de>
- [6] S. Jaeckel, L. Raschkowski, K. Börner, and L. Thiele, "QuaDRiGa: A 3-D multi-cell channel model with time evolution for enabling virtual field trials," *IEEE Trans. Antennas Propag.*, vol. 62, pp. 3242–3256, 2014.
- [7] L. Raschkowski, S. Jaeckel, F. Undi, L. Thiele, W. Keusgen, B. Pitakdumrongkija, and M. Ariyoshi, "Directional propagation measurements and modeling in an urban environment at 3.7 GHz," *Proc. ACSSC '16*, pp. 1799–1803, 2016.
- [8] M. Peter, K. Sakaguchi *et al.*, "H2020-ICT-671650-mmMAGIC/D2.1: Measurement campaigns and initial channel models for preferred suitable frequency ranges," Tech. Rep., 2016.
- [9] 3GPP TR 37.885 v15.2.0, "Study on evaluation methodology of new vehicle-to-everything v2x use cases for lte and nr," Tech. Rep., 2018.
- [10] 3GPP TR 38.811 v15.0.0, "Study on new radio (NR) to support non terrestrial networks," Tech. Rep., 2018.
- [11] 3GPP TR 36.777 v15.0.0, "Study on enhanced LTE support for aerial vehicles," Tech. Rep., 2017.
- [12] B. Fleury, M. Tschudin, R. Heddergott, D. Dahlhaus, and K. Inge-man Pedersen, "Channel parameter estimation in mobile radio environments using the sage algorithm," *IEEE J. Sel. Areas Commun.*, vol. 17, no. 3, pp. 434–450, 1999.
- [13] S. Jaeckel, "Quasi-deterministic channel modeling and experimental validation in cooperative and massive MIMO deployment topologies," Ph.D. dissertation, TU Ilmenau, 2017. [Online]. Available: https://www.db-thueringen.de/receive/dbt_mods_00032895
- [14] N. Jaldén, P. Zetterberg, B. Ottersten, and L. Garcia, "Inter-and intrasite correlations of large-scale parameters from macrocellular measurements at 1800 MHz," *EURASIP J. Wireless Commun. Netw.*, no. 2007:025757, 2007.